MODELING A SOLAR-HYBRID MICRO GAS TURBINE

Brian Ssebabi[1], Frank Dinter[2] and Johan van der Spuy[3]

[1] Solar Thermal Energy Research Group (STERG), Department of Mechanical and Mechatronic Engineering, Stellenbosch University, Private Bag X1, Matieland 7602, South Africa; Phone: +27738675945; Email: brianssebabi@sun.ac.za

[2] Solar Thermal Energy Research Group (STERG), Department of Mechanical and Mechatronic Engineering, Stellenbosch University; E-Mail: frankdinter@sun.ac.za

[3] Solar Thermal Energy Research Group (STERG), Department of Mechanical and Mechatronic Engineering, Stellenbosch University; E-mail: sjvdspuy@sun.ac.za

Abstract

This paper models the performance of a solar-hybrid micro gas turbine (MGT) under real solar thermal conditions, and predicts its performance for up to 15 kW distributed electricity generation solar-hybrid applications in Southern Africa. The gas generator of the MGT is based on a BorgWarner Turbo Systems turbocharger (Manufacturer: KKK Serial no. 504064262), and the operating range of the MGT is restricted by that of the turbocharger. Initially, a standard twin shaft MGT Brayton cycle – without solar thermal input - was modeled, to determine the system fuel requirement, specific fuel consumption, net power output and overall cycle efficiency. Thereafter, a twin shaft MGT system incorporating a solar thermal input was modeled, and the effect of the solar thermal input on the overall MGT system performance was investigated. The system fuel mass flow required to maintain the pre-set turbine inlet temperature decreased with increase in solar thermal input. Adding a solar receiver to the standard twin shaft MGT system resulted in a reduction in the pressure ratio available to the power turbine, which in turn led to a reduction in the system power output and cycle thermal efficiency. Additional MGT components also result in an increase in the non-dimensional mass flow of the power turbine and a reduction in the pressure ratio available to the power turbine, which necessitates designing a power turbine with the ability to operate at higher non-dimensional mass flows and lower pressure ratios.

Keywords: Micro gas turbine; Solar-hybrid micro gas turbine; Solar-hybrid micro gas turbine modeling.

1. Introduction

Southern Africa is blessed with one of the best solar energy resources worldwide – receives an annual DNI in excess of 2100 kW/m^2 [1], and the solar-hybrid concept offers a viable option for both a reduction in over reliance on fossil fuel energy resources and an avenue for exploitation of the available renewable energy resource.

Solar-hybrid power systems based on gas turbines combine solar energy and fossil fuel, and thus provide reliable power with full dispatchability. Central receiver tower solar-hybrid power systems take advantage of the very high concentration ratios of central receiver tower technology to achieve a high receiver outlet air temperature. The high receiver outlet air temperature ensures a reduction in the amount of back-up fuel combusted to raise the air temperature to the required turbine inlet temperature.

The development of solar-hybrid gas turbine systems has been ongoing for several decades, with more focus on solar components, and less focus on the gas turbine systems themselves [2].

Some of the earliest research work relating to the application of MGTs (less than 350 kW) in solar-hybrid power systems was performed by [3]. The MGT was based on a turbocharger, and the aim was to estimate the performance and component costs for a proposed 30 kWe dish/Brayton solar-hybrid engine. An estimated thermal-to-electric efficiency of 30% and levelized electricity costs (LEC) comparable to those of a 25 kWe dish/Stirling system were obtained.

The European Commission (EC) previously funded three solar-hybrid driven gas turbine research projects: SOLar hybrid GAs Turbine Electric (SOLGATE) power system, SOLar-HYbrid power and COgeneration (SOLHYCO) plants and SOLar Up-scale GAs turbine System (SOLUGAS). The main objective of these research projects was to demonstrate the performance and cost reduction potential of solar-hybrid driven gas turbine systems, with the focus on improvement in receiver design and development [4, 5 and 6]. The SOLGATE and SOLHYCO projects demonstrated the practical usage of a solar-hybrid MGT based on a modified helicopter 250 KW turboshaft engine, and a maximum electricity output of 230 kW, at a cycle efficiency of 20% was realised [7, 8, 9 and 10].

This paper models a solar-hybrid MGT based on a turbocharger, for distributed electricity generation solar-hybrid applications in Southern Africa. The turbocharger is commercially available and it has a compressor wheel of diameter 95 mm and a turbine wheel of diameter 86 mm. The

original equipment manufacturer (OEM) [11] provided turbocharger total-to-static test data, and this data was plotted as compressor and turbine performance maps (see Figures 2 and 3). These maps were then used to determine the operating range of the MGT. It has to be noted that no suitable design has been completed for the power turbine, therefore there are no performance maps available for the power turbine.

Typical compressor and turbine performance maps can be found in [12]. The compressor maps plot the compressor total-to-total pressure ratio P_{02}/P_{01} and isentropic efficiency $\eta_{c,t-t}$ against the non-dimensional mass flow rate $\dot{m}\sqrt{T_{01}}/P_{01}$, along each constant speed line $N/\sqrt{T_{01}}$, while the turbine maps plot the turbine non-dimensional mass flow rate $\dot{m}\sqrt{T_{03}}/P_{03}$ and total-to-static efficiency $\eta_{t,t-s}$ against the total-to-static pressure ratio P_{03}/P_4, along each constant speed line $N/\sqrt{T_{03}}$. Similarly, the power turbine maps plot $\dot{m}\sqrt{T_{04}}/P_{04}$ and $\eta_{tp,t-s}$ against P_{04}/P_5 along each constant speed line $N_p/\sqrt{T_{04}}$. In these equations, the suffixes 1 and 2 denote the gas generator compressor inlet and outlet conditions, 3 and 4 denote the gas generator turbine inlet and outlet conditions and 4 and 5 denote the power turbine inlet and outlet conditions (as shown in Figure 1). The suffix 0 denotes stagnation (total) conditions.
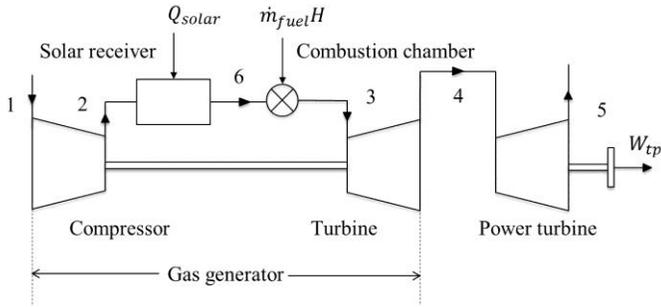
Fig. 1. Schematic layout of a solar-hybrid MGT Brayton cycle with a twin shaft arrangement

The use of off-the-shelf automotive turbocharger technology ensures a simple and modular structure, easy usage and low cost of the turbomachinery. The modular and simple structure design of the MGT makes it suitable for concentrating solar power (CSP) distributed electricity generation applications in Southern Africa.

An important consideration for a MGT constructed from an off-the-shelf turbocharger is the shaft arrangement. A twin shaft arrangement – with a gas generator and a mechanically independent (free) power turbine - was chosen (see Figure 1), mainly because it allows for flexibility of operation, which is necessary given the variable nature of the solar energy resource. The twin shaft arrangement has an added advantage of ease of starting compared with a single shaft arrangement, as the starter needs to only turn over the gas generator.

2. Modeling approach

The modeling of the MGT system was done in MATLAB. Initially, a standard twin shaft MGT system - with no solar thermal input - was modeled, to determine the system fuel mass flow, specific fuel consumption, thermal energy input and overall cycle efficiency. Thereafter, a twin shaft MGT system incorporating a solar thermal input into the compressed air was modeled, and the effect of the solar thermal input on the overall MGT system performance was investigated.

2.1. Solar resource

The heliostat field was modeled based on Stellenbosch University's Helio100 test facility at Mariendahl. Helio100 has a heliostat field aperture area of 267.6 m[2].

Hourly averaged direct normal irradiance (DNI) for the 4th August, 2016 was downloaded from the Sonbesie weather station website [13]. The weather station uses a Kipp and Zonen (K&Z) CHP1 pyrheliometer (calibrated on 18th July, 2012) to directly measure the DNI.

To determine the solar thermal output from the heliostat field Q_{solar}, the optical efficiency of the heliostat field $\eta_{optical}$ was first determined, using a sixth order polynomial that takes into consideration shading, blocking and cosine effects [14]

$$\eta_{optical} = 0.4245\theta_z^6 - 1.148\theta_z^5 + 0.3507\theta_z^4 + 0.755\theta_z^3 - 0.5918\theta_z^2 + 0.0816\theta_z + 0.832 \tag{1}$$

where θ_z is the zenith angle, and can be calculated from the declination angle, hour angle and the solar altitude angle, following a procedure given by [15].

The solar thermal output from the field was then calculated using

$$Q_{solar} = \eta_{optical} \times \eta_{reflect,avail,soil,track} \times A_{field\ aperture} \times DNI \tag{2}$$

where $\eta_{reflect,avail,soil,track}$ is a heliostat efficiency, and combines factors like heliostat reflectivity, availability, soiling and tracking accuracy. It was assumed to be 81 per cent, as suggested by [15].

The solar receiver was modeled based on the cluster of pressurised air receivers tested during the SOLGATE project. The receiver modeling followed an approach similar to that of [16] and [17]. A linear correlation between the efficiency of the receiver cluster and the temperature of the compressed air at the receiver outlet T_{06} was obtained for the receiver test data found in [4], as given below

$$\eta_{rec} = 1.1279 - 0.00034T_{06} \tag{3}$$

Equation 3 was then used in combination with the calculated solar thermal output from the solar field (Equation 2) to determine the temperature of the compressed air at the
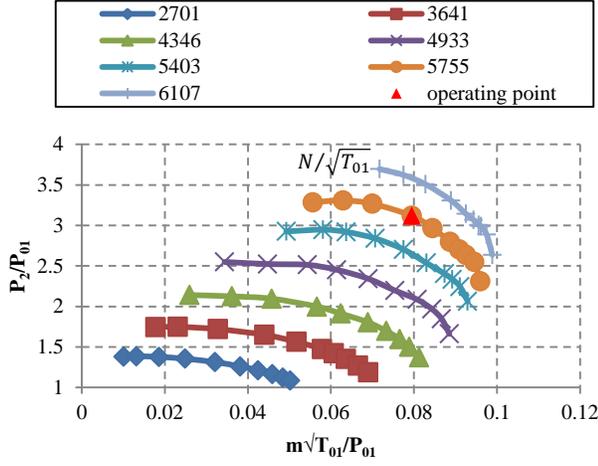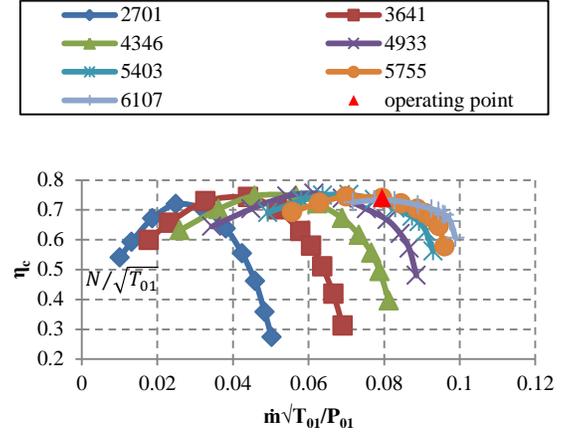
Fig. 2. Gas generator compressor operating point: (a) pressure ratio vs non-dimensional mass flow and (b) isentropic efficiency vs non-dimensional mass flow

receiver outlet and subsequently, the solar thermal input into the compressed air. The compressed air temperature at the receiver outlet was then raised to the pre-set turbine inlet temperature T_{03}, of 800 ^{0}C – restricted by turbine blade metallurgical limitations - by combusting additional fuel.

The solar receiver was assumed to have a constant pressure drop of 2 per cent of the compressor delivery pressure, as was measured across the receiver cluster in [4].

Other simplifying assumptions made during the modeling include:

- Assume constant total ambient conditions of 101.325 kPa and 293 K

- Assume a constant mass flow throughout the system, neglecting increase in mass flow due to the fuel mass flow (since the fuel mass flow is normally less than 2 per cent of the air mass flow)

- Neglect system inlet and outlet pressure losses

- The specific heat at constant pressure c_p and consequently the specific heat ratio γ is a function of temperature alone, over the working range of pressure and temperature

- The model uses Propane as fuel, with a calorific value $H = 46.3$ MJ/kg

- The power turbine is assumed to have an isentropic efficiency of 85 per cent and mechanical efficiency of 99 per cent

- Assume a constant combustion chamber pressure drop of 7 per cent of the compressor delivery pressure and combustion efficiency of 95 per cent

2.2. Modeling procedure

The modeling procedure was as follows: Select a constant speed line on the compressor map and choose a compressor operating point (see Figure 2), with care taken to select an operating point; a sufficient distance away from the compressor

surge line (extreme left of each constant speed line), at a relatively high compressor pressure ratio, and in a region of high compressor isentropic efficiency. Selecting a high compressor pressure ratio accommodates system pressure losses that result from incorporating additional components like a solar receiver, recuperator, *et cetera* into the MGT system. The values of P_2/P_{01}, $\dot{m}\sqrt{T_{01}}/P_{01}$, $N/\sqrt{T_{01}}$ and $\eta_{c,t-s}$, can then be determined for the selected compressor operating point, as given below in Table 1:

Table 1. Selected compressor operating point parameters

Parameter	Value
P_2/P_{01}	3.1192
$\dot{m}\sqrt{T_{01}}/P_{01}$	0.0795
$N/\sqrt{T_{01}}$	5755
$\eta_{c,t-s}$	0.7391

The air mass flow rate $\dot{m}$ and the compressor rotation speed N are determined from $\dot{m}\sqrt{T_{01}}/P_{01}$ and $N/\sqrt{T_{01}}$, given the known ambient conditions at the compressor inlet P_{01} and T_{01}. The static pressure at the compressor outlet P_2 is determined from P_2/P_{01}, while the static temperature at the compressor outlet T_2 is determined from P_2/P_{01} and $\eta_{c,t-s}$. First, the static isentropic temperature at the compressor outlet T_{2s} is calculated using the ideal gas isentropic relation between pressure and temperature ratios

$$T_{2s} = T_{01}\left(\frac{P_2}{P_{01}}\right)^{(\gamma-1)/\gamma} \tag{4}$$

and then the determined T_{2s} is substituted into Equation 2, with the known η_c and T_{01}, to obtain T_2

$$T_2 = T_{01} + \frac{T_{2s} - T_{01}}{\eta_{c,t-s}} \tag{5}$$
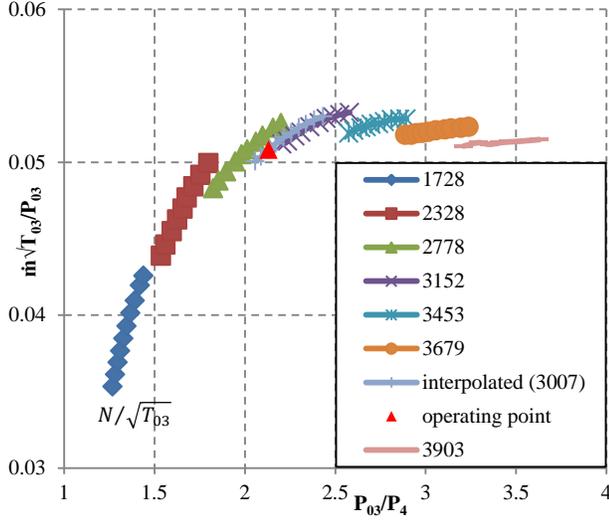
(a)
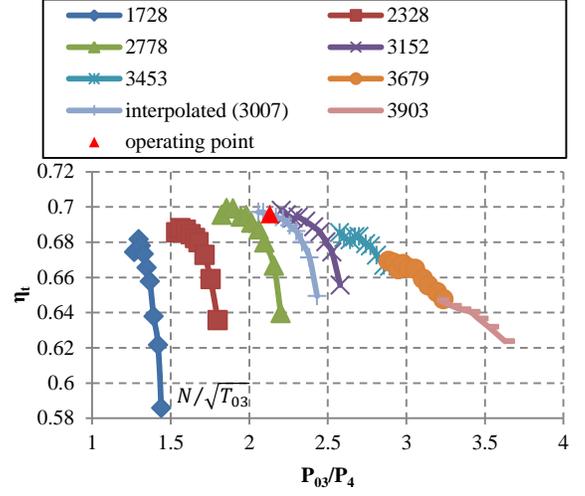
(b)

Fig. 3. Gas generator turbine operating point: (a) non-dimensional mass flow vs pressure ratio and (b) isentropic efficiency vs pressure ratio

The stagnation temperature at the compressor outlet T_{02} is then calculated using

$$T_{02} = T_2 + \frac{V_2}{2c_p} \qquad (6)$$

where V_2 is the compressed air velocity at the compressor outlet, and is given by

$$V_2 = \frac{\dot{m}RT_2}{P_2 \pi d_2^2/4} \qquad (7)$$

R is the molar gas constant and d_2 is the pipe diameter at the compressor outlet. The stagnation pressure at the compressor outlet P_{02} is then determined from the calculated P_2, T_2 and T_{02}, using the ideal gas isentropic relation between pressure and temperature ratios

$$P_{02} = P_2 \left(\frac{T_{02}}{T_2}\right)^{\gamma/(\gamma-1)} \qquad (8)$$

The gas generator inlet pressure P_{03} is then determined from the difference between the determined P_{02} and the pressure drop across the combustor, and any other additional components like the solar receiver, recuperator, *et cetera*. The work requirement of the compressor W_c is then determined from the temperature rise in the compressor $\Delta T_{012} = T_{02} - T_{01}$, using

$$W_c = \dot{m}c_p \Delta T_{012} \qquad (9)$$

The gas generator turbine parameters $N/\sqrt{T_{03}}$ and $\dot{m}\sqrt{T_{03}}/P_{03}$ can then be calculated from the determined P_{03} and N, and the corresponding P_{03}/P_4 and η_t read from the gas generator turbine characteristic (see Figure 3). This ensures speed and flow compatibility between the gas generator compressor and turbine operating points.

The static pressure at the gas generator turbine outlet P_4 is then determined from P_{03}/P_4, using the known P_{03}, while the static temperature at the gas generator turbine outlet (power turbine inlet) T_4 is determined from P_{03}/P_4, and $\eta_{t,t-s}$. First, the static isentropic temperature at the gas generator turbine outlet T_{4s} is calculated using the ideal gas isentropic relation between pressure and temperature ratios and then the determined T_{4s} is substituted into Equation 10, with the known $\eta_{t,t-s}$ and T_{03}, to obtain T_4

$$T_4 = T_{03} - \eta_{t,t-s}(T_{03} - T_{4s}) \qquad (10)$$

The stagnation temperature at the gas generator turbine outlet T_{04} is then calculated using

$$T_{04} = T_4 + \frac{V_4}{2c_p} \qquad (11)$$

where V_4 is the gas stream velocity at the gas generator outlet, and is given by

$$V_4 = \frac{\dot{m}RT_4}{P_4 \pi d_4^2/4} \qquad (12)$$

d_4 is the pipe diameter at the gas generator turbine outlet. The stagnation pressure at the gas generator turbine outlet P_{04} is then determined from the calculated T_4 and T_{04}, using the ideal gas isentropic relation between pressure and temperature ratios

$$P_{04} = P_4 \left(\frac{T_{04}}{T_4}\right)^{\gamma/(\gamma-1)} \qquad (13)$$

The gas generator turbine work W_t is then determined from the temperature drop in the gas generator turbine $\Delta T_{034} = T_{03} - T_{04}$, using

$$W_t = \eta_{mec}\dot{m}c_p\Delta T_{034} \qquad (14)$$

To ensure work compatibility between the gas generator compressor and turbine, $W_c \approx W_t$.

The power turbine parameters $\dot{m}\sqrt{T_{04}}/P_{04}$ and P_{04}/P_5 can thereafter be calculated from the now known $\dot{m}$, T_{04} and P_{04}, while P_5 is assumed to be equal to the ambient pressure, as the power turbine exhausts to the atmosphere. If the power turbine maps are available, the power turbine parameters $N/\sqrt{T_{04}}$ and η_{tp}, corresponding to the calculated $\dot{m}\sqrt{T_{04}}/P_{04}$ and P_{04}/P_5 can thereafter be read from the power turbine maps, thus ensuring flow matching between the gas generator turbine and the power turbine.

Similar to the gas generator turbine, the power turbine exhaust stagnation temperature T_{05} can be determined from P_{04}/P_5 and $\eta_{tp,t-s}$. The power output of the power turbine W_{tp} can similarly be determined from the temperature drop in the power turbine $\Delta T_{045} = T_{04} - T_{05}$.

To determine the system fuel mass flow required to raise the temperature of the air to the preset turbine inlet temperature T_{03}, the combustion chamber inlet stagnation temperature needs to first be determined. For the standard twin shaft MGT system, the combustion chamber inlet stagnation temperature is equal to the stagnation temperature at the compressor outlet T_{02} while with a solar thermal input into the compressed air, the combustion chamber inlet stagnation temperature is equal to the solar receiver outlet stagnation temperature T_{06}, which is in turn dependent on the solar thermal output of the heliostat field. First, the receiver efficiency is alternatively defined as the ratio of the solar thermal energy transferred to the compressed air to the solar thermal output from the heliostat field, as given by

$$\eta_{rec} = \frac{\dot{m}c_p(T_{06} - T_{02})}{Q_{solar}} \qquad (15)$$

Then equating Equations 3 and 15, T_{06} can be determined from

$$T_{06} = \frac{1.1279 + \dfrac{\dot{m}c_p T_{02}}{Q_{solar}}}{\dfrac{\dot{m}c_p}{Q_{solar}} + 0.00034} \qquad (16)$$

The system fuel mass flow $\dot{m}_f$ is then determined from performing an energy and mass balance for the combustion chamber, using
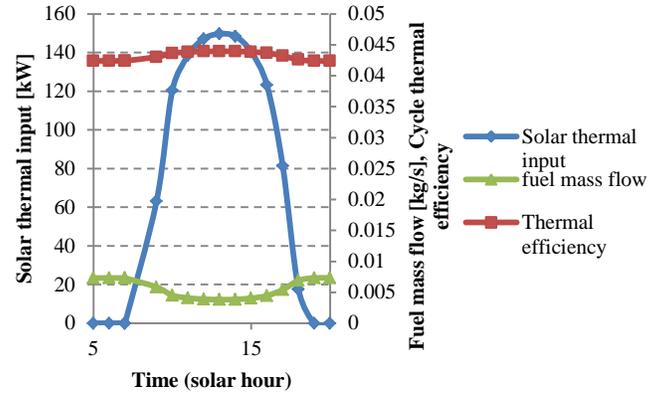
Fig. 4. Effect of solar thermal input on the system fuel mass flow and thermal efficiency

$$\dot{m}_f = \frac{\dot{m}c_p(T_{03} - T_{06})}{(H - c_p T_{03})} \qquad (17)$$

The system specific fuel consumption SFC is then determined from

$$SFC = \frac{3600\dot{m}_f}{W_{tp}} \qquad (18)$$

Finally, the overall cycle thermal efficiency η is determined from the ratio of the power output W_{tp} to the overall system thermal input Q_{th}

$$\eta = \frac{W_{tp}}{Q_{th}} \qquad (19)$$

where for a solar thermal input into the compressed air

$$Q_{th} = \dot{m}_f H + \dot{m}c_p(T_{06} - T_{02}) \qquad (20)$$

5. Results

For the standard twin shaft MGT, the calculated fuel mass flow was 0.0073 kg/s, corresponding to a specific fuel consumption of 0.0012 kg/Wh. The net power output was 22.1 kW, for an overall cycle thermal efficiency of 6.5%. For the solar-hybrid MGT, the solar receiver outlet temperature increased from 450.15 K to 754.18 K, and this in turn led to a decrease in the fuel mass flow from 0.0073 to 0.0038 kg/s (see Figure 4), corresponding to a decrease in the specific fuel consumption from 0.0018 to 0.0010 kg/Wh. The calculated net power output was 14.4 kW, at a maximum cycle thermal efficiency of 4.4%, for the period with solar thermal input.

A comparison of the power turbine characteristic (non-dimensional mass flow and pressure ratio) for the MGT without and with solar thermal input shows an increase in the non-dimensional mass flow from 0.0934 to 0.1011, corresponding to pressure ratios of 1.5126 and 1.3915, respectively.

5. Discussion and conclusion

This paper models the operation of a MGT under real solar thermal conditions, and predicts its performance for solar-hybrid applications in Southern Africa. The system fuel mass flow required to maintain the pre-set turbine inlet temperature decreased with increase in solar thermal input, leading to a reduction in the specific fuel consumption. The integration of a solar receiver (and any other additional components) into the MGT system led to an increase in the overall system pressure drop which in turn resulted in a decrease in the pressure ratio that is available to the power turbine. The reduction in pressure ratio resulted in a decrease in the power output, which in turn led to a decrease in the overall cycle efficiency. The overall cycle efficiency can be increased by improving the efficiencies of the individual MGT components. Also, incorporating recuperation would reduce the amount of fuel combusted to raise the air temperature to the required turbine inlet temperature, but would in turn increase the system pressure drop.

The modeling of the solar-hybrid MGT showed an increase in the power turbine non-dimensional mass flow with the addition of a solar receiver. The non-dimensional mass flow parameter is an indication of the swallowing capacity of the power turbine, which in turn restricts the operating range of the gas generator turbine upstream of the power turbine. Additional MGT components result in an increase in the non-dimensional mass flow of the power turbine and a reduction in the pressure available to the power turbine. This necessitates designing a power turbine with the ability to operate at higher non-dimensional mass flows and lower pressure ratios

Acknowledgements

References

[1] P. Gauche, T. W. von Backstrom and A.C. Brent, A concentrating solar power value proposition for South Africa, Journal of Energy in Southern Africa, vol. 24, no. 1 (2013).

[2] J. Spelling, B. Laumert, T. Fransson, Optimal Gas-Turbine Design for Hybrid Solar Gas-Turbine Power Plant Operation, Transactions of the ASME, Journal of Engineering for Gas-Turbines and Power, Volume 134/9, (2012).

[3] D.R. Gallup, J.B. Kesseli, A solarized Brayton engine based on turbocharger technology and the DLR receive, Intersociety Energy Conversion Engineering Conference, Monterey, CA (United States), (1994).

[4] European Commission, SOLGATE Solar hybrid gas turbine electric power system. Final Publishable Report ISBN 92-894-4592-0, (2005).

[5] European Commission, Solar-Hybrid Power and Cogeneration Plants, Public report, (2011).

[6] R. Korzynietz, M. Quero and R. Uhlig, SOLUGAS-Future solar hybrid technology, in SolarPACES Conference, Marrakech, (2012).

[7] A. Ring, C. Sugarmen, J. Sinai, R. Buck, P. Schwarzbozl, P. Heller, T. Denk, J. Fernandez and F. Tellez, Solar Powered Gas Turbine Prototype – Technology Development and Test Results, PowerGen Europe, Barcelona, (2004).

[8] U. Fisher, C. Sugarmen, A. Ring and J. Sinai, Gas Turbine "Solarization" – Modifications for Solar/Fuel Hybrid Operation, Transactions of the ASME, Journal of Solar Energy Engineering, vol. 126, (2004).

[9] J. Sinai, C. Sugarmen and U. Fisher, Adaptation and Modification of Gas Turbines for Solar Energy Applications, Proceedings of GT2005 ASME Turbo Expo, (2005).

[10] P. Heller, M. Pfander, T. Denk, F. Tellez, A. Valverde, J. Fernandez and A. Ring, Test and Evaluation of a Solar Powered Gas Turbine System, Solar Energy 80, pp. 1225-1230, (2006).

[11] Tom Heuer, BorgWarner Turbo Systems Engineering GmbH, Email communication, (2016).

[12] H. I. H. Saravanamuttoo, G. F. C. Rogers, H. Cohen and P. V. Straznicky, (2009) Gas Turbine Theory – 6th ed., Pearson Education Limited, Essex, pp. 184 and pp. 365.

[13] http://weather.sun.ac.za/downloadList.php (Accessed on 5th August, 2016)

[14] P. Gauche, S. Pfenninger, A. J. Meyer, T. W. von Backstrom and A.C. Brent, Modeling dispatchability potential of CSP in South Africa, Southern African Solar Energy Conference, (2012).

[15] Stine, W. and Geyer, M. (2001) 'Power from the Sun', [online] Available from: http://www.powerfromthesun.net/book.htm (Accessed on 1st August, 2016)

[16] Heller, L. and Gauché, P., Dual-pressure Air Receiver Cycle for Direct Storage Charging, Energy Procedia, 49, pp. 1400–1409, (2014).

[17] C. Homann, Effects of solar hybridization on the performance of a gas turbine, Masters Thesis, Stellenbosch University, (2015).